Journal of Associated Medical Sciences 2023; 56 (1): 141-149

JAMS
Journal of Associated Medical Sciences

Scopus indexed & Thai-Journal Citation Index Centre (TCI)

Journal of Associated Medical Sciences

Journal homepage: https://www.tci-thaijo.org/index.php/bulletinAMS/index

Hepatic lesion detectability in abdomen computed tomography: Investigation in low kVp single energy and low keV virtual monochromatic images generated from dual energy computed tomography using task-based image quality assessment in phantom

Hataipat Jantawong* **Anchali Krisanachinda**

Faculty of Medicine, Chulalongkorn University, Bangkok, Thailand.

ARTICLE INFO

Article history:
Received 24 June 2022
Accepted as revised 18 October 2022
Available online 14 November 2022

Keywords:
Low tube potential single energy CT, dual-energy CT imaging, virtual monochromatic image, task-based image quality assessment, detectability index, hepatic lesion detectability, abdomen CT imaging

ABSTRACT

Background: Low tube potential single-energy (SE) and virtual monochromatic image (VMI) dual energy (DE) abdomen CT images both improve the hepatic lesion detection by increasing the liver lesion contrast on images.

Objectives: To study the performance of low kVp single energy and low keV virtual monochromatic images (VMI) generated from dual energy acquisition to detect the hepatic lesion on abdominal CT imaging in phantom.

Materials and methods: The anthropomorphic liver with nodule inserted phantom with extension rings simulating the small, medium, and large patient was scanned under the SECT acquisition by varying the kVp from 70-120 kVp and for DECT acquisitions, three kVp combinations (80/-,90/-, and 100/Sn150-kVp). The series of 40-,50-,60-, and 70-keV VMI were generated from DECT data set. All images were used to assess the task-based image quality; task transfer function (TTF), noise power spectrum (NPS), and detectability index (d') with the diagnostic task to detect 15 mm diameter hyperattenuating hepatic lesion.

Results: The result showed that the TTF was higher in low kVp SECT while the lesion contrast was higher at low keV VMI -DECT. The noise magnitude remained constant for all kVp values in SECT, but it was dramatically increased as decreased the energy level from 70- to 40-keV in VMI-DECT. The f_{av} of NPS shifted to higher frequency when increasing the kVp and when increasing the energy level of VMI. The obtained d' was highest in low kVp SECT at 70-or 80-kVp.

Conclusion: The low kVp SECT provided the highest d' than that in low keV VM image from DECT in all phantom sizes where the highest d' was found at 70 kVp-SECT for small and medium phantom and at 80 kVp for large phantom. For SECT, reduced the kVp to 70- or 80-kVp improved the detectability index. The kVp combination in DECT impacts to the d' of VMI; at small phantom, the highest d' for each keV VMI was found at 80/Sn150 kVp acquisition and at larger phantom size, higher kVp on tube "A" is more favored.

* **Corresponding author.**
Author's Address: *Faculty of Medicine, Chulalongkorn University, Bangkok, Thailand.*
E-mail address: j.hataipat@gmail.com
** **doi:** 10.12982/JAMS.2023.029
E-ISSN: 2539-6056

Introduction

Primary liver cancer is the sixth most-commonly diagnosed cancer and the third leading cause of cancer related death worldwide in 2020.[1] Hepatocellular carcinoma (HCC) is the most common type of primary liver cancer comprising of 75-85% of cases. In current clinical practice, CT is commonly used as an imaging modality for accurate detection and characterization of liver tumors.[2-4] Therefore, the lower noise images and multiphase acquisition are required to detect small hepatic lesions.

The low tube potential (low kVp) technique has been introduced to improve the conspicuity of liver lesion in appropriate patient size and reduce the radiation dose to patient in clinical abdomen CT.[5,6] However, this technique can be challenged in large patient because the X-ray attenuation is more and thus requires increasing of mAs to maintain the image quality. Unfortunately, the greater increase in mAs may not be achievable in some CT system due to inherent engineering design that limits in maximum X-ray output at lower kVp.

Recently, dual-energy computed tomography (DECT) is considered a promising new development in CT that had a potential to improve detection an d characterization of liver lesion.[7,8] The introduction of third generation dual source dual energy CT system provided several new improvement features; a new 150 kVp for high voltage tube equipped with thicker tin (Sn) filter enables an improvement of spectral separation, higher X-ray tube current to overcome the limitation of maximum mA at low-kVp or ultra-high pitch settings. Therefore, possible kV combinations in this generation are generally at 80/Sn150, 90/Sn150, and 100/Sn150.

Lesion detectability can be assessed using task-based image quality with the human observer or mathematical model observer method. The detectability index (d') which is a task-based detection performance metric based on mathematical model observer, has been introduced and implemented for the assessment of low-contrast detectability in modern CT systems.[9-11] This metric can be quantified using of non-pre-whitening observer model with eye filter (NPWE) that incorporated the resolution in term of task transfer function (TTF), noise texture, diagnostic task, and viewing conditions.

The purpose of this study is to investigate the lesion detectability for small hepatic lesion in abdominal CT images acquiring at low-kVp single energy and low keV VM image from dual energy acquisition. The impact of different kVp in SECT and different kV combination in DECT was also investigated for various sizes of phantom.

Materials and methods

A. Phantom study

An oval shape semi-anthropomorphic liver nodule phantom (QRM Moehrendorf, Germany) with size of 300x200x100 mm in x-, y-, and z- dimensions, was used t quantify task-based image quality and detectability inde of hepatic lesion. The two extension rings with mediu and large sizes with outside diameters on X- and Y-axes o 350x250 mm and 400x300 mm respectively, were adde to closely simulate the larger patient habitus (Figure 1a). This phantom is comprised of the abdomen body wit respect to the density typically 35 HU +/- 5 HU at 120 kV. The liver part has CT No. approximately 90 HU at 120 kVp, containing the hyperdense liver nodules with the CT No. approximately 180 HU at 120 kVp. This contributes the liver and nodule contrast at approximately 90 HU at 120 kVp scan. The phantom was placed at the isocenter for each CT acquisition.

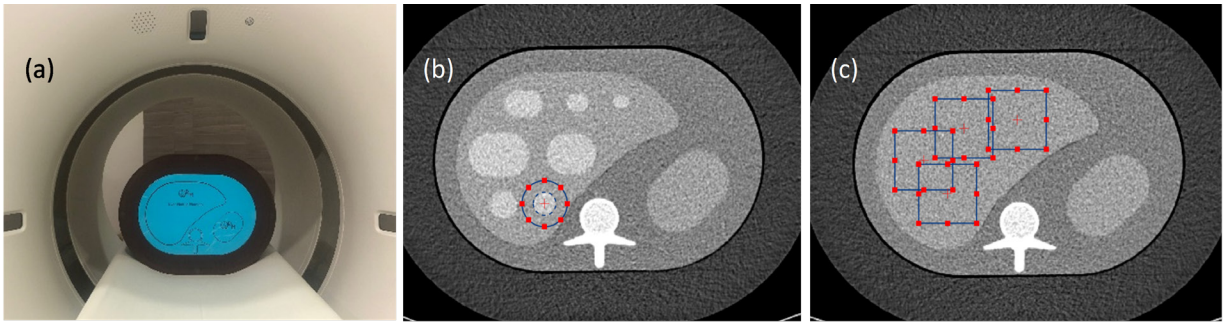

Figure 1 *Set up for phantom study. (a): liver nodule phantom equipped with the large extension ring (size L) placed at isocenter of CT scanner, (b): circular ROI placed on the 20 mm liver nodule insert to measure the TTF, (c): four-square ROIs were placed on the uniform area of liver phantom.*

B. CT Image acquisition and reconstruction parameters

The phantom was scanned by the third generation dual-source CT scanner (Somatom® Force, Siemens Healthineers, Forcheim, Germany). The acquisition parameters of abdominal CT protocol were used as listed in Table1. In this study, we aim to compare the benefits of using low kVp single energy and low keV VMI dual energy -CT acquisition in term of image quality and detectability based on clinical indication for hepatic lesion detection. The kVp values were varied from 70-120 kVp with 10 kVp interval and 120 kVp was defined as the reference kVp. For dual energy acquisition, three kVp-combinations were used: 80/Sn150, 90/Sn150, and 100/Sn150 kVp. The tube current modulation was activated to take account for elliptical shape of phantom in abdomen CT. The volumetric dose index ($CTDI_{vol}$) for 32 cm body phantom of each imaging protocol was recorded both for single and dual energy acquisitions.

The phantom was scanned 3 times for each acquisition and reconstructed into axial images using advanced modeled iterative reconstruction (ADMIRE) with strength 2. The standard soft tissue reconstruction kernel (Br36 for SECT and Qr36 for DECT) was used with the slice thickness of 0.6 mm and reconstruction field of view (FOV) fit to the scanned phantom of 320, 360 and 420 mm for small, medium, and large phantom size respectively.

Table 1 Acquisition and reconstruction parameters for abdomen single and dual energy CT protocols.

Acquisition mode	Single energy (SE)	Dual energy (DE)		
kVp setting	80, 90, 100, 110, 120	80/Sn150	90/Sn150	100/Sn150
Tube current modulation	On	On		
Quality reference mAs (A/B)	300	500*/250	350*/250	3600*/150
Rotation time	0.5	0.5		
Pitch	0.6	0.6		
Slice acquisition	192x0.6 mm	128x0.6 mm		
Reconstruction method	ADMIRE (2)	ADMIRE (2)		
Reconstruction Kernel	Br 36	Qr 36		

Note: For DECT acquisition, Quality reference mAs was adjusted only for tube "A", tube "B" was automatically computed by the system.

The reconstructed images of low- and high- kVp from DECT data were transferred to Syngo.via software, Siemens, Healthineer. The virtual monochromatic images (VMI) were generated at 40, 50, 60, and 70 keV using the "Monoenergentic+" function which is based on the image-based algorithm in Syngo Dual Energy application.

C. Task-based image quality assessment

In this study, the task-based image quality was assessed by using the imQuest software, version 7.1, designed by Duke Clinical Imaging Physics Group (Duke University).[9] The software assessed spatial resolution using the task transfer function (TTF), noise magnitude and texture using the noise power spectrum (NPS), and to estimate the ability of radiologist to detect specific lesions by using detectability index (d'). The specific clinical task in this study is to detect the small hepatocellular carcinoma (HCC) which is the hyperattenuating lesions in liver.

The TTF was assessed by placing the circular ROI on 20 mm hyperdense liver nodule in phantom image (Figure 1b). According to the methodology, 5 consecutive slices of axial image were used to compute the edge spread function (ESF) and then line spread function (LSF). Finally, by taking the Fourier Transform (FT) of LSF, TTF curve can be carried out.[9] Like the modulation transfer function (MTF), TTF curves can be summarized by the spatial frequencies at which the TTF reaches 50%, denoted as f_{50}.

The NPS was computed by placing four-square ROIs on the uniform area of liver region in phantom images (Figure 1c). The NPS curve was generated with the following equation[11]

$$NPS_{2D}(f_x, f_y) = \frac{\Delta_x \Delta_y}{L_x L_y} \frac{1}{N_{ROI}} \sum_{i=1}^{N_{ROI}} |FT_{2D}\{ROI_i(x,y) - \overline{ROI_i}\}|^2$$

where Δ_x and Δ_y are the pixel sizes in the x- and y-dimension, L_x and L_y are the ROI's lengths in pixel for both x- and y-dimensions, N_{ROI} is the number of ROIs used, $(\overline{ROI_i})$ is the mean pixel value averaged from $ROI_i\ (x,y)$. The NPS curves obtained from the measurement were used to quantify the noise magnitude by taking a square root of the area under the NPS curve, the noise texture by reporting the peak frequency, f_p, and the average NPS spatial frequency, f_{av}.

Combining the resolution (TTF) and noise (NPS) properties of the image with the predefined clinical imaging task (W) together, the detectability index (d') was then computed. The detectability index based on non-prewhitening observer model with eye filter (d'_{NPWE}) was computed for a predefined clinical task as follows:

$$d'^2_{NPWE} = \frac{[\iint |W_{task}(u,v)|^2 \cdot TTF^2(u,v) \cdot E(u,v)^2 dudv]^2}{\iint |W_{task}(u,v)|^2 \cdot TTF^2(u,v) \cdot NPS(u,v) \cdot E(u,v)^4 dudv}$$

where u and v are the spatial frequencies in the x-and y-directions, E the eye filter that models the human visual system sensitivity to different spatial frequencies, and W(u,v) the task function. The detection of small HCC task was assumed to represent the circular signal with a 15 mm diameter. The software computed the d' under the interpretation condition of 1.5 zoom factor and a viewing distance of 500 mm.

Results

Task-based image quality from images acquired for 70-120 kVp SECT and 40-70 keV-VMI acquired from DECT with varying the kVp combination; 80/Sn150,90/Sn150 and 100/Sn150 kVp were obtained for various size of phantom under tube current modulation as shown in Table 2. $CTDI_{vol}$ from each acquisition were collected for three phantom sizes and the values were shown in Table 3. The $CTDI_{vol}$ increased as the phantom size increased. The $CTDI_{vol}$ obtained from low kVp-SECT and the DECT scan mode were lower than that from a conventional 120 kVp scan in all phantom sizes.

Table 2 Summary of task-based image quality.

		SECT (kVp)						VMI-DECT (keV)				
		70	80	90	100	110	120		40	50	60	70
Small	Noise magnitude (HU)	20.09	20.27	19.78	19.84	20.04	18.56	80/Sn150	39.81	28.77	22.14	18.11
								90/Sn150	42.99	30.98	23.78	19.41
								100/Sn150	45.85	33.04	25.32	20.63
	$f_{av}(mm^{-1})$	0.22	0.22	0.23	0.23	0.22	0.23	80/Sn150	0.21	0.22	0.22	0.23
								90/Sn150	0.22	0.22	0.23	0.23
								100/Sn150	0.22	0.23	0.23	0.23
	$f_{peak}(mm^{-1})$	0.16	0.19	0.17	0.17	0.17	0.17	80/Sn150	0.11	0.17	0.17	0.17
								90/Sn150	0.11	0.19	0.20	0.20
								100/Sn150	0.16	0.16	0.16	0.16
	$f_{50}(mm^{-1})$	0.39	0.33	0.38	0.36	0.35	0.30	80/Sn150	0.22	0.22	0.22	0.23
								90/Sn150	0.27	0.26	0.27	0.27
								100/Sn150	0.23	0.25	0.27	0.28
	d'	49.80	43.82	41.64	38.72	35.21	40.88	80/Sn150	30.63	33.90	35.96	36.41
								90/Sn150	27.96	30.54	32.19	32.29
								100/Sn150	26.43	27.78	30.35	30.56
	CNR	5.78	4.91	4.74	4.38	4.13	4.55	80/Sn150	5.04	5.05	4.87	4.68
								90/Sn150	4.41	4.41	4.32	4.20
								100/Sn150	4.51	4.00	3.77	3.52
Medium	Noise magnitude (HU)	22.73	23.75	23.97	24.69	24.56	24.41	80/Sn150	47.69	34.38	26.44	21.55
								90/Sn150	51.08	36.54	27.82	22.55
								100/Sn150	52.67	37.73	28.74	23.27
	$f_{av}(mm^{-1})$	0.20	0.21	0.22	0.22	0.22	0.22	80/Sn150	0.20	0.21	0.21	0.21
								90/Sn150	0.20	0.21	0.22	0.22
								100/Sn150	0.20	0.21	0.22	0.22
	$f_{peak}(mm^{-1})$	0.14	0.16	0.17	0.16	0.17	0.17	80/Sn150	0.08	0.09	0.14	0.16
								90/Sn150	0.06	0.16	0.16	0.16
								100/Sn150	0.08	0.16	0.16	0.17
	$f_{50}(mm^{-1})$	0.31	0.31	0.30	0.35	0.34	0.33	80/Sn150	0.22	0.23	0.23	0.24
								90/Sn150	0.20	0.21	0.21	0.22
								100/Sn150	0.19	0.19	0.20	0.20
	d'	35.80	31.50	33.21	32.41	27.35	29.81	80/Sn150	17.14	18.94	22.19	22.00
								90/Sn150	18.09	19.85	21.34	21.36
								100/Sn150	21.79	25.35	29.35	30.69

Table 2 Summary of task-based image quality. (continued)

		SECT (kVp)						VMI-DECT (keV)				
	CNR	4.98	4.15	3.70	3.53	3.42	3.40	80/Sn150	3.38	3.29	3.40	3.22
								90/Sn150	3.53	3.39	3.22	3.04
								100/Sn150	4.40	4.25	4.08	3.89
Large	Noise magnitude (HU)	27.80	26.29	26.48	26.45	27.42	27.60	80/Sn150	52.54	37.73	28.82	23.41
								90/Sn150	56.07	39.98	30.30	24.43
								100/Sn150	57.15	40.74	30.86	24.85
	$f_{av}(mm^{-1})$	0.19	0.20	0.20	0.21	0.21	0.22	80/Sn150	0.18	0.19	0.20	0.20
								90/Sn150	0.19	0.20	0.20	0.21
								100/Sn150	0.18	0.19	0.20	0.21
	$f_{peak}(mm^{-1})$	0.13	0.14	0.14	0.14	0.16	0.17	80/Sn150	0.06	0.09	0.16	0.16
								90/Sn150	0.06	0.08	0.14	0.14
								100/Sn150	0.06	0.06	0.13	0.13
	$f_{50}(mm^{-1})$	0.30	0.26	0.27	0.32	0.25	0.25	80/Sn150	0.22	0.22	0.23	0.25
								90/Sn150	0.06	0.08	0.14	0.14
								100/Sn150	0.06	0.06	0.13	0.13
	d'	23.89	25.39	21.61	19.82	19.73	20.30	80/Sn150	12.05	13.94	15.69	16.22
								90/Sn150	15.59	16.51	18.74	19.38
								100/Sn150	11.52	14.13	17.49	20.34
	CNR	3.78	3.51	3.10	2.94	2.34	2.48	80/Sn150	2.83	2.88	2.86	2.71
								90/Sn150	3.54	3.31	3.39	3.31
								100/Sn150	2.99	3.09	3.17	3.26

*Note: *NPS, TTF at 50% (f_{50}), d' and conventional image quality metric (CNR), obtained from the images acquired for 70-120 kVp SECT and 40-70 keV-VMI from DECT with varying the kVp combination; 80/Sn150, 90/Sn150, and 100/Sn150 kVp in small, medium, and large phantom.*

Table 3 Radiation dose from different kVp in SECT and different kVp combination in DECT scan for small, medium, and large phantom size is displayed in $CTDI_{vol}$ (mGy).

	Single Energy						Dual Energy		
	120 kVp*	70 kVp	80 kVp	90 kVp	100 kVp	110 kVp	80/Sn150	90/Sn150	100/Sn150
Small	**10.44**	8.98	8.56	8.53	8.57	8.41	8.79	8.46	8.26
Medium	**14.45**	12.36	12.98	12.85	12.68	12.5	12.48	12.5	13.38
Large	**20.31**	17.62	16.93	16.85	16.4	16.43	17.04	17.3	18.11

A. Task transfer function (TTF)

For SECT acquisition, as the kVp is increasing, f_{50} shifted toward the lower frequency in small and large phantom sizes and shifted toward the higher frequency in medium phantom size. For DECT acquisition, f_{50} shifted to higher frequency as energy level of VMI increased in all kVp-combinations. The higher of f_{50} was observed in low kVp in SECT image compared to low keV- VMI in DECT for all phantom sizes where to be found at 70 kVp-SE in small phantom and at 100 kVp-SE in medium and large phantom. With increasing the phantom size, f_{50} shifted toward a lower frequency at low kVp-SECT (70-110 kVp). The shift of f_{50} toward to lower frequency as increased the phantom size was also founded in low energy VMI-DECT at 90/Sn150 and 100/Sn150 kV combination while the f_{50} remains constant for all phantom sizes in VMI images generated from 80/Sn150 kVp scan. The resulting lesion to liver background contrast in HU from different scanning condition was also displayed. Then compared to 120 kVp SECT, lesion contrast gradually improved as reduced the kVp in SECT while it was dramatically improved at low keV VMI in DECT especially at 40- and 50-keV in all phantom sizes.

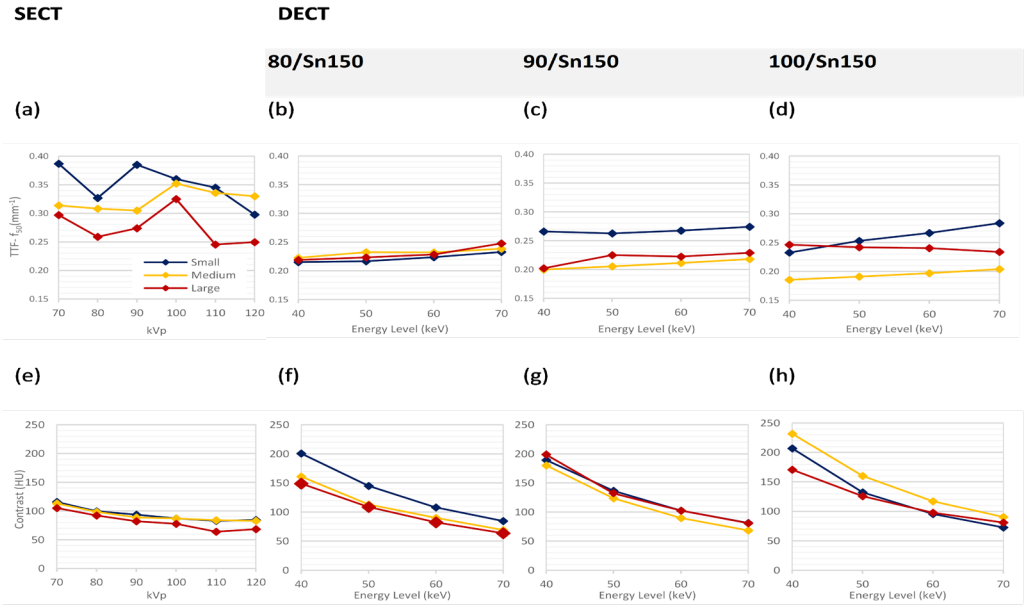

Figure 2 *The 50% TTF values and contrast in HU obtained from different scanning conditions for SECT and DECT acquisitions for small ,medium and large phantom. The top row is 50% TTF (f_{50}) values for (a) 70-120 kVp-SECT scan and for the 40-70 keV images from (b) 80/Sn150, (c) 90/Sn150 kVp and (d) 100/Sn150 kVp combination. in DECT scan. The bottom row is contrast (HU) values for (e) 70-120 kVp-SECT scan and for 40-70 keV images from (f) 80/Sn150 kVp,(g) 90/Sn150 kVp and (h) 100/Sn150 kVp combination in DECT scan.*

B. Noise power spectrum (NPS)

The noise magnitude (HU) increased with increasing the phantom size, however it remained constant in all kVp settings of SECT within a same phantom size. For VMI-DECT images, the noise magnitude gradually decreased by approximately 55% as energy level increased from 40 to 70 keV. The effect of kVp combination shown as an increased of noise magnitude (in all energy levels) as increased the kVp in low-kVp tube from 80/Sn150 to 100/Sn150. In term of the noise texture, the average NPS spatial frequency (f_{av}) shifted toward the lower frequency when reduced the kVp from 120- to 70-kVp or when increased the phantom size from small to large. In low keV-VMI generated from DECT scan, the f_{av} shifted toward the lower frequency when lowering of energy level from 70-to 40-keV and when the phantom size increased from small to large. The changing in of kVp combination slightly impact to the f_{av}, by the f_{av} was slightly increased as changing the kVp combination from 80/-to 100/Sn150 kVp as shown in Figure 3 (a-h).

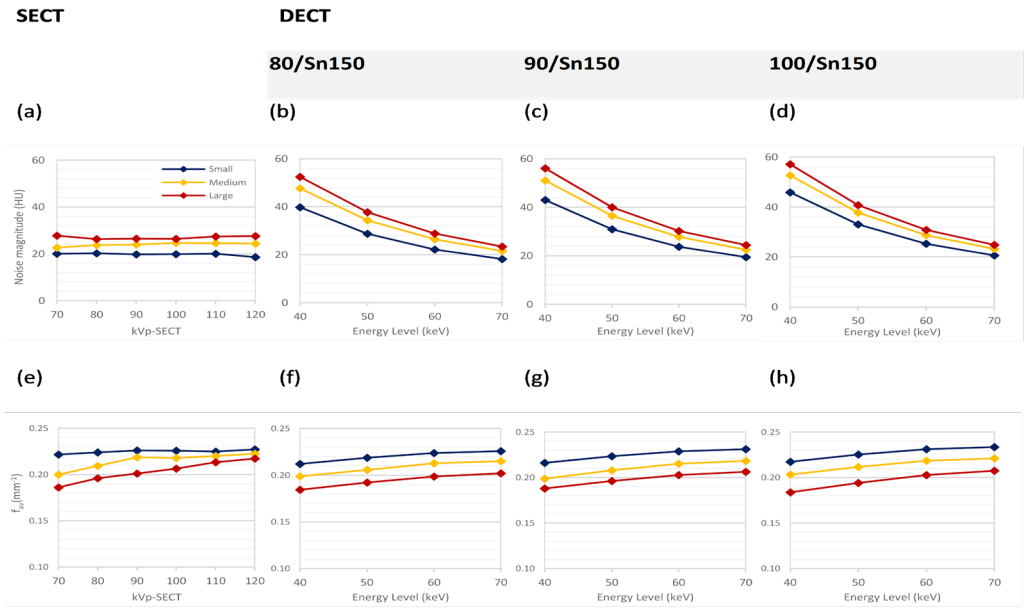

Figure 3 *Noise magnitude (HU) and average NPS spatial frequency (f_{av}) obtained from different scanning conditions for SECT and DECT acquisitions for small ,medium and large phantom. The top row is the noise magnitude (HU) obtained for (a) 70-120 kVp-SECT scan and for the 40-70 keV images from (b) 80/Sn150, (c) 90/Sn150 kVp, and (d) 100/Sn150 kVp combination in DECT scan. The bottom row is the average NPS spatial frequency (f_{av}) obtained for (e) 70-120 kVp-SECT scan and for 40-70 keV images from (f) 80/Sn150 kVp, (g) 90/Sn150 kVp and (h) 100/Sn150 kVp combination in DECT scan.*

C. Detectability index (d')

The detectability index (d') was computed based on the task of detection for 15 mm hyper-attenuation liver lesion.The d' estimated for images acquired using different kVp-SECT and low keV VMI-DECT, the obtained d' values were shown in Figure 4. The images obtained from low kVp-SECT scan at 70-, 80-, and 90-kVp yielded the higher d' compared to 120 kVp scan and d' decreased as phantom size increased. The highest d' was found for image obtained at 70 kVp for small and medium phantom size and at 80 kVp for large phantom size. On the contrary, as reduced the energy level from 70- to 40-keV of VMI in DECT, the d' decreased. At small phantom size, the d' was found to be highest at 80/Sn150 kVp compared to others. At the medium phantom size, the highest d' was found at 100/Sn150 kVp but at large phantom size, the highest d' was at 90/Sn150 kVp. Comparing between low kVp SECT and low keV-VMI DE scan, the d' was higher for low kVp-SECT scan in all phantom sizes.

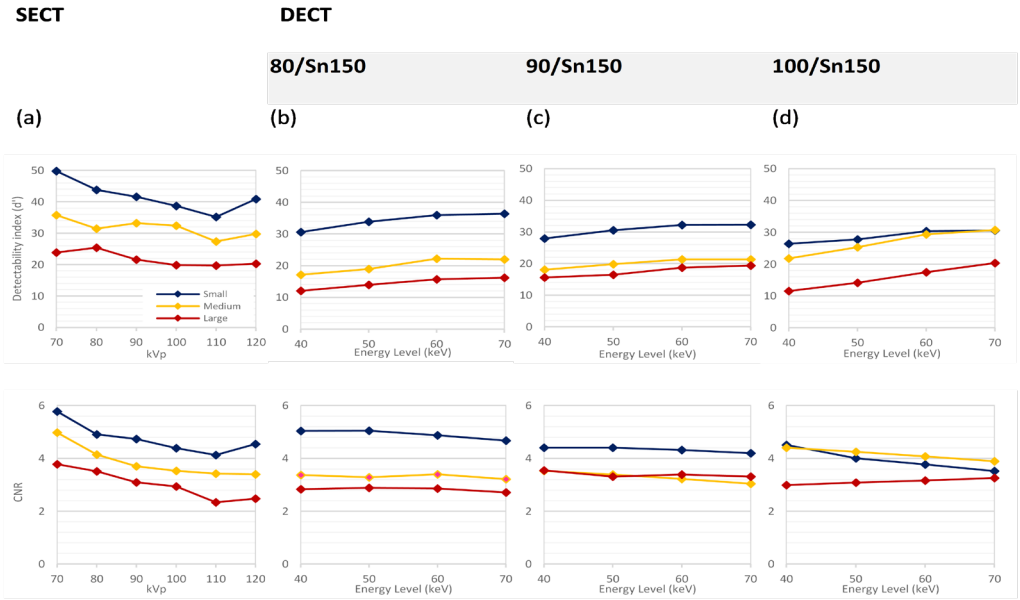

Figure 4 *Detectability index (d') and contrast to noise ratio (CNR) from different scanning conditions for SECT and DECT. The top row was d' values obtained from (a) 70-120 kVp-SE in all phantom sizes, the 40-70 keV images from (b) 80/Sn150, (c) 90/Sn150 and (d) 100/Sn150 kVp combination in DECT for small , medium and large phantom. The bottom row was CNRs obtained from (e) 70-120 kVp-SECT scan and for the 40-70 keV images from (f) 80/Sn150, (g) 90/Sn150 and (h) 100/Sn150 kVp combination in DECT.*

Discussion

This study performed to investigate the lesion detectability for small hepatic lesion in abdomen CT images acquiring at low kVp-SECT and low keV VMI-DECT on anthropomorphic liver nodules phantom under clinical protocol with tube current modulations. The clinical task in our study was defined as the detection of a 15 mm hyperattenuating hepatic lesion based on the typical lesion size that small HCC is usually detected in CT examination[7,12] and this size is in a range of clinically important to an effective treatment outcomes of HCC.[13,14] Our results demonstrated that the liver to lesion contrast (HU) was improved by reducing the kVp in SECT or by lowering the energy level (40-60 keV) of VMI in DECT according to increase of photoelectric interaction in low energy x-ray beam and complied with many studies.[5-7, 12] In this study the automatic tube current (mA) modulation was activated for all scanning protocols to take account with various sizes of phantom which the mA was modulated with the reference mAs at 120 kVp for standard patient size. Figure 3a demonstrated the excellent performance of the automatic mA modulation system in this scanner to maintain the image quality (noise) among the different kVp within the same phantom size. Therefore, the noise magnitude in this study was not affected by the kVp selection in SECT but for the synthetic images of VMI in DECT was not the same. The noise magnitude was dramatically increased as decreased the energy level of VMI especially at 40- and 50- keV for all phantom sizes. The impact of kVp combination shown as slightly increase of noise magnitude when increasing the kVp at tube "A" from 80 to 100 kVp. The f_{av} of NPS shifted toward the lower frequency imply to the shape of noise texture changed and demonstrated as image smoothness. In this study, the f_{av} shifted to the lower frequency was found in medium and large phantom sizes when reduced to lower kVp in SECT. This phenomenon was described by the study of Solomon *et al.* the manufacturer has implemented statistical weighting of the raw data into their iterative reconstruction algorithms which is more aggressive in low-signal condition (i.e., low dose or large phantom), the image will consist of slightly more low-frequency content and then visualized as larger grains compared to smaller phantom.[15]

The spatial resolution of images in this study was quantified using task transfer function (TTF). The further the TTF shifted toward lower frequencies, the larger spatial resolution reduction. For TTF, the circular edge technique had been used to plot the ESF and the ESF was influenced

by the image noise and the contrast between liver nodule inserted and liver phantom background, which these two are impacted as a function of kVp used in SECT or keV level of VMI in DECT as well as the kVp combination used and phantom size. Our study showed that the highest 50% TTF (f_{50}) was found at 70 kVp SECT in small phantom and at 100 kVp in SE in medium and large phantom corresponding to the high contrast and low noise settings.

The detectability index is a method of non-pre-whitening observer model with eye filter (NPWE) that incorporated the resolution, noise texture, diagnostic task, and 2D viewing conditions, changes of only one of these factors influenced the d'. The investigation of d' for various scanning conditions will be clinically benefit to the radiologist and technologist as guided for proper selection of scan and reconstruction parameters to achieve targeted diagnostic task on each examination. In our study, if the detection of 15 mm heperattenuation hepatic lesion was the primary diagnostic task, the scanning at 70 kVp-SECT is suitable for small and medium phantom and at 80 kVp-SECT for the large phantom size. Our result corresponds to the study of Hansan *et al*.[7] which reported higher lesion CNRs and higher radiologist preference scores in low kVp-SECT than that in 40-50 keV-VMI even though the lesion conspicuity (reflect to high lesion contrast) is high in low keV VMI-DE. However, if the dual energy acquisition is clinically required for small patient size, selection of 80/Sn150 kVp combination is most appropriate due to yielding the highest d' and 100/Sn150 kVp is preferred to improve the d' for larger patient. This was confirmed by the study of Michalak *et al*.[16] conducted for different phantom sizes .

This study demonstrated that using the low kVp SECT and low keV-VMI have potential on improvement of hepatic lesion detection in CT while reduce the radiation dose to patient compared to 120-kVp SECT scan. When compared the d' to 120 kVp scan, the higher d' values were mostly observed in low kVp SECT (70-100 kVp) rather than from low keV-VMI from DECT scan for all phantom sizes due to better image resolution and lower image noise in SECT images. However, at medium and large phantoms size, using 70 keV-VMI at 100/Sn150 resulting to comparable d'. This inferred that the utilizing the DECT in larger patient may add up the benefits on increase the diagnostic confidence to radiologist from additional image types generated from DECT data set such as virtual non contrast images (VNC), iodine images, iodine quantification, etc. without deterioration of lesion detection and dose penalty.

There are some limitations on this study which was carried out using the institutional abdomen imaging protocol at the standard acquisition scanning and single reconstruction parameter. The other parameters further from the kVp in SECT and keV combination in DECT along with various phantom sizes have not been investigated. Moreover, the variation on morphology of lesions (i.e., different lesion size or lesion contrast), have not been carried out. The hyperdense liver nodules in anthropomorphic abdomen phantom used in this study simulated the attenuation property of 90 HU liver nodule at 120 kVp scan, did not include iodine-based material, resulted in the deviation from the clinical study. However, this methodology has been accepted by multiple researchers who studied on d' of liver lesion in CT based on acrylic insert in image quality phantom.[17-20] To the knowledge from this study that the d' of low keV VMI is inferior to that from the low-kVp SECT acquisition, the further study should be conducted to study the impact of DECT parameters on d' that may help to improve the d' on VMI images in the future. The phantom study included more clinical lesions is required to add more information relevant to our results.

Conclusion

The lesion detectability for small hepatic lesion in abdominal CT images acquiring at low-kVp single energy and low keV VM image from dual energy acquisition were investigated. The highest d' was found at 70 kVp-SECT for small and medium phantom and at 80 kVp for large phantom. For SECT, reduced the kVp to 70- or 80-kVp improved the detectability index. For DECT, increased the energy level of VMI from 40-70 keV improved the d' in all phantom sizes. The kVp combination in DECT impacts the d' of VMI; at small phantom the d' values for each keV VMI was highest at image acquired from 80/Sn150 kVp and at larger phantom size, higher kVp on tube "A" is more favored.

Acknowledgements

The authors would like to thank the Department of Radiology, King Chulalongkorn Memorial Hospital, for providing instruments in this research and Ratchadapiseksompotch Fund, Faculty of Medicine, Chulalongkorn University, grant number RA63/068 for research funding.

Conflict of interest

The authors have no relevant conflicts of interest to disclose.

Ethic approval

This study was performed on phantom, therefore this research was qualified with an exemption on the ethic committee approval.

References

[1] Sung H, Ferlay J, Siegel RL, Laversanne M, Soerjomataram I, Jemal A, et al. Global Cancer Statistics 2020: GLOBOCAN Estimates of Incidence and Mortality Worldwide for 36 Cancers in 185 Countries. CA Cancer J Clin. 2021; 71(3): 209-49.

[2] Choi JY, Lee JM, Sirlin CB. CT and MR imaging diagnosis and staging of hepatocellular carcinoma: part II. Extracellular agents, hepatobiliary agents, and ancillary imaging features. Radiology. 2014; 273(1): 30-50.

[3] Marrero JA, Kulik LM, Sirlin CB, Zhu AX, Finn RS, Abecassis MM, et al. Diagnosis, Staging, and Management of Hepatocellular Carcinoma: 2018 Practice Guidance by the American Association for the Study of Liver Diseases. Hepatology. 2018; 68(2): 723-50.

[4] Kim DW, Choi SH, Kim SY, Byun JH, Lee SS, Park SH, et al. Diagnostic performance of MRI for HCC according to contrast agent type: a systematic review and meta-analysis. Hepatol Int. 2020; 14(6): 1009-22.

[5] Ehman EC, Guimarães LS, Fidler JL, Takahashi N, Ramirez-Giraldo JC, Yu L, et al. Noise reduction to decrease radiation dose and improve conspicuity of hepatic lesions at contrast-enhanced 80-kV hepatic CT using projection space denoising. Am J Roentgenol. 2012; 198(2): 405-11.

[6] Lv P, Liu J, Chai Y, Yan X, Gao J, Dong J. Automatic spectral imaging protocol selection and iterative reconstruction in abdominal CT with reduced contrast agent dose: initial experience. Eur Radiol. 2017; 27(1): 374-83.

[7] Hanson GJ, Michalak GJ, Childs R, McCollough B, Kurup AN, Hough DM, et al. Low kV versus dual-energy virtual monoenergetic CT imaging for proven liver lesions: what are the advantages and trade-offs in conspicuity and image quality? A pilot study. Abdom Radiol (NY). 2018; 43(6): 1404-12.

[8] Lee YJ, Lee JM, Lee JS, Lee HY, Park BH, Kim YH, et al. Hepatocellular carcinoma: diagnostic performance of multidetector CT and MR imaging-a systematic review and meta-analysis. Radiology. 2015; 275(1): 97-109.

[9] Samei E, Bakalyar D, Boedeker KL, Brady S, Fan J, Leng S, et al. Performance evaluation of computed tomography systems: summary of AAPM task group 233. Med Phys. 2019; 46(11): e735-e56.

[10] Chen B, Christianson O, Wilson JM, Samei E. Assessment of volumetric noise and resolution performance for linear and nonlinear CT reconstruction methods. Med Phys. 2014; 41(7): 071909.

[11] Verdun F, Racine D, Ott J, Tapiovaara M, Toroi P, Bochud F, et al. Image quality in CT: From physical measurements to model observers. Physica Medica. 2015; 31(8): 823-43.

[12] Shuman WP, Green DE, Busey JM, Mitsumori LM, Choi E, Koprowicz KM, et al. Dual-energy liver CT: effect of monochromatic imaging on lesion detection, conspicuity, and contrast-to-noise ratio of hypervascular lesions on late arterial phase. Am J Roentgenol. 2014; 203(3): 601-6.

[13] Choi JY, Lee JM, Sirlin CB. CT and MR imaging diagnosis and staging of hepatocellular carcinoma: part I. Development, growth, and spread: key pathologic and imaging aspects. Radiology. 2014; 272(3): 635-54.

[14] Thun M, Linet MS, Cerhan JR, Haiman CA, Schottenfeld D. Cancer epidemiology and prevention: Oxford University Press; 2017.

[15] Solomon J, Wilson J, Samei E. Characteristic image quality of a third generation dual-source MDCT scanner: Noise, resolution, and detectability. Med Phys. 2015; 42(8): 4941-53.

[16] Michalak G, Grimes J, Fletcher J, Halaweish A, Yu L, Leng S, et al. Selection of optimal tube potential settings for dual-energy CT virtual mono-energetic imaging of iodine in the abdomen. Abdom Radiol (NY). 2017; 42(9): 2289-96.

[17] Greffier J, Si-Mohamed S, Dabli D, de Forges H, Hamard A, Douek P, et al. Performance of four dual-energy CT platforms for abdominal imaging: a task-based image quality assessment based on phantom data. Eur Radiol. 2021; 31(7): 5324-34.

[18] Greffier J, Frandon J, Sadate A, Akessoul P, Belaouni A, Beregi JP, et al. Impact of four kVp combinations available in a dual-source CT on the spectral performance of abdominal imaging: A task-based image quality assessment on phantom data. J Appl Clin Med Phys. 2021; 22(8): 243-54.

[19] Cester D, Eberhard M, Alkadhi H, Euler A. Virtual monoenergetic images from dual-energy CT: systematic assessment of task-based image quality performance. Quant Imaging Med Surg. 2022; 12(1): 726.

[20] Solomon J, Wilson J, Samei E. Characteristic image quality of a third generation dual-source MDCT scanner: Noise, resolution, and detectability. Med Phys. 2015; 42(8): 4941-53.